I&EC research
Industrial & Engineering Chemistry Research

Article

Cite This: Ind. Eng. Chem. Res. 2019, 58, 12280−12290

pubs.acs.org/IECR

Designing High-Performance Nanofiltration Membranes for High-Salinity Separation of Sulfate and Chloride in the Chlor-Alkali Process

Qian Wang,[†,‡,§] Yue Wang,[†,‡,§] Bo-Zhi Chen,[†,‡,§] Tian-Dan Lu,[†,‡,§] Han-Lin Wu,[†,‡,§] Yi-Qun Fan,[†,‡,§] Weihong Xing,[†,‡,§] and Shi-Peng Sun*[,†,‡,§]

[†]State Key Laboratory of Materials-Oriented Chemical Engineering, [‡]Jiangsu National Synergetic Innovation Center for Advanced Materials, and [§]College of Chemical Engineering, Nanjing Tech University, Nanjing 211816, China

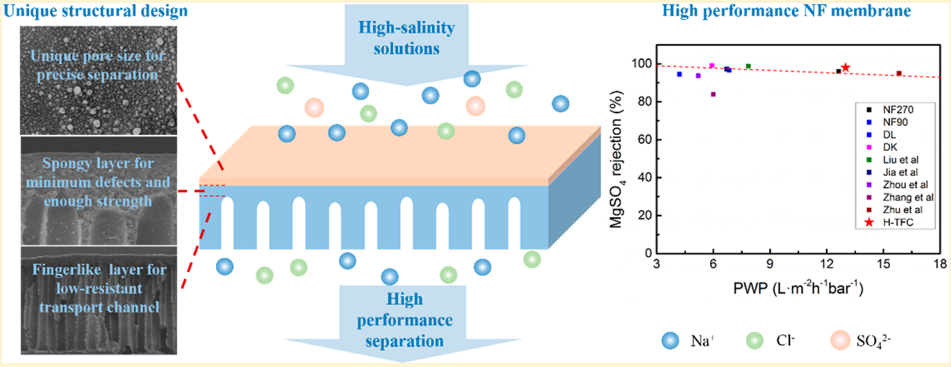

ABSTRACT: Enormous demand exists for separation of high-salinity solutions across various industries, especially in those high-pollution businesses which are urgently looking for high-throughput and precise-selective nanofiltration (NF) membranes stably operating at elevated concentrations and other harsh environments. This work develops a novel NF membrane (i.e., high-performance thin-film composite (H-TFC)) through straightforward structure design instead of complex post-treatment to achieve high performance during high-salinity separation of sulfate and chloride ions. Through manipulating dope composition and coagulation bath temperature, unique macro- and microstructures of the H-TFC membrane were designed: (1) The substrate possesses the best ratio of the spongy and fingerlike layers, which not only provides low resistance transport channels to improve the membrane permeability (13.0 L m^{2-} h^{-1} bar^{-1}) but also ensures enough strength and minimum defects to treat high-salinity solutions. (2) The unique nominal pore size (0.364 nm) of the finely tuned selective layer can realize the separation of Cl^- and SO_4^{2-} at relatively high level (separation factor about 9000). The excellent long-term stability and resistance toward chlorine and heat grant the H-TFC membranes great potential for application in high-salinity solution separation of chlor-alkali and other industries.

1. INTRODUCTION

High-salinity solutions are abundant in many factories, such as pharmaceutical, petroleum, chemical, textile, food-processing, and leather industries.[1] It should be properly treated before utilized or discharged. Otherwise, it may cause severe damage on soil microorganisms, mineral balance and, aquatic life, due to the high concentrations of chlorides and sulfates.[2] The chlor-alkali industry is one of the most typical processes which uses high-salinity solutions (concentrated NaCl solution) to produce sodium hydroxide and chlorine.[3−5] It is significant for the chlor-alkali industry that NaCl and Na_2SO_4 of a high-salinity solution should be separated to achieve resource recycling and reduce harmful effects.[6] Nowadays, various physical and chemical methods have been designed over the years, such as chemical precipitation, ion exchange, crystallization, and purging.[7−10] However, these methods are high cost, environmentally unfriendly, or difficult to implement.[11] Apparently, efficient treatment of high-salinity solutions must be achieved with a green and effective technology to lower the cost and pollution. As a pressure-driven separation technology based on size exclusion and Donnan exclusion, nanofiltration (NF) has become a promising method, due to its high retention of multivalent anion salts, low retention of monovalent ions, low investment, flexibility of the process, and environmental friendliness.[12,13]

NF membrane performs under the joint action of steric (size-exclusion) effects, electrostatic (Donnan exclusion) partitioning interactions between the external solution and the membrane, and dielectric exclusion, with unique narrow pore size distribution, and charged characteristics,[14,15] which provide it great potential in sulfate and chloride separation.

Received: April 24, 2019
Revised: June 4, 2019
Accepted: June 7, 2019
Published: June 7, 2019

DOI: 10.1021/acs.iecr.9b02217
Ind. Eng. Chem. Res. 2019, 58, 12280−12290

Nevertheless, treatment of the high-salinity solutions in the chlor-alkali process demands a great anti-attenuation membrane capacity both in physical and chemical aspects.[16] Thus, an ideal NF membrane for high-salinity separation of NaCl and Na_2SO_4 should possess: (1) a robust and highly porous substrate to avoid performance attenuation caused by compression and concentration polarization of high concentration feed solution; (2) a highly selective top layer with excellent resistance toward chlorine, heat for long-term stability.

According to previous studies, various methods have been adopted to enhance compressive strength of membranes, such as using robust material,[17−21] adding inorganic particles,[22−24] cross-linking polymer chain,[25,26] and so on. Wang and co-workers prepared NF hollow fiber membrane by using polybenzimidazole as raw material.[27] The obtained membrane with compressive strength owns long-term stability in forward osmosis (FO) system. Yang and co-workers improved compressive strength of polysulfone (PSF) membrane by adding nanosized TiO_2 particles into the dope.[28] The mechanism of changing the compressive property by mixing inorganic particles and polymer was investigated, and the results were proved by XRD and DSC analysis. Sun and co-workers fabricated a NF membrane by hyperbranched polyethylenimine (PEI)-induced cross-linking on a polyamide−imide hollow fiber support.[29] The resulted membrane can keep sufficient compressive strengths under high pressure. With respect to chlorine resistance, Cheng and co-workers investigated chlorine attacking thin-film composite (TFC) mechanism that the active amidic hydrogen linking to aromatic ring can be attacked by chlorine easily, which results to the destruction of TFC.[30]

However, the NF membranes for separation of high-salinity solutes are still underdeveloped. Existing membranes are prone to attenuation of flux and selectivity due to improper design of the composite structure. Therefore, the main objective of this work is to develop an optimum NF membrane through designing the substrate structure. First, the influence of the dope composition and bath temperature upon construction of the substrate is studied under the guidance of thermodynamics and dynamics during the phase transformation process. Normally, the substrates fabricated through non-solvent-induced phase separation (NIPS) are typically combined with a spongelike layer and a macrovoid layer. Fingerlike macrovoids may work as porous transport channel to improve the membrane permeability as well as reduction of internal concentration polarization. The spongy layer can enhance the compressive strength to resist membrane compression and minimize defects that may cause inefficient separation. Thus, we designed the best ratio of the spongelike layer and the macrovoid layer to improve membrane properties. Second, piperazine (PIP) was selected as diamine monomer in the interfacial polymerization, which was chosen for its secondary amine. According to the above two strategies, a high-performance NF membrane, which is denoted as H-TFC, was prepared. The rejection of $MgSO_4$ was above 98%, and the pure water flux can reach 78 L m^{-2} h^{-1} when the operation pressure was 6 bar under cross-flow operation. Moreover, the sulfate ion rejection of H-TFC membrane was more than 98%, and there was almost no interception of chloride ions in the separation experiment of the sodium sulfate and sodium chloride. Compared with the commercial DL membrane (SUEZ, US), H-TFC membrane obtained a higher flux under high salinity operation, which indicates its great potential in chlor-alkali and other industries for high-salinity solution separation and wastewater treatment.

2. EXPERIMENTAL SECTION

2.1. Materials. Commercially available poly(ether sulfone) (PES, Solvay) was used to prepare the membrane substrate. *N*-Methyl-2-pyrrolidone (NMP, 99.0%), *N*,*N*-dimethylacetamide (DMAc, AR-grade) and *N*,*N*-dimethylformamide (DMF, AR-grade) were employed as solvents, while polyethylene glycol (PEG 400, AR-grade) were acquired as additive of dope solutions for fabricating the membrane substrate. The solvents and PEG 400 were all purchased from Sinopharm Chemical Reagent Co., Ltd. (Sinopharm, China). Piperazine (PIP, >99.5%, Sinopharm), trimesoyl chloride (TMC, >98.0%, Aladdin), and *n*-hexane (>97.0%, Aladdin) were employed to perform interfacial polymerization. Inorganic salts, including sodium sulfate (Na_2SO_4, AR-grade), magnesium sulfate ($MgSO_4$, AR-grade), magnesium chloride ($MgCl_2$, AR-grade), and sodium chloride (NaCl, AR-grade) were purchased from Sinopharm China to test NF performance.

2.2. Fabrication of PES Membrane Substrates. Asymmetric polymeric substrates were synthesized using the NIPS process. First, PES powder was dried in a vacuum oven at 90 °C overnight to remove moisture. A certain ratio of PES and PEG-400 was then dissolved in a certain solvent and stirred at 50 °C for 12 h to form a homogeneous solution, which was then set aside for 12 h to eliminate air bubbles trapped in the solution. The dopes were then cast into membranes with a 100 μm thick casting knife on nonwoven fabrics. The phase transition process was then carried out in DI water bath. The as-prepared substrate was afterward repeatedly washed with DI water to remove the remaining solvent and stored in DI water until use.

2.3. Fabrication of TFC Membranes. Thin polyamide (PA) selective layers were deposited on substrates via interfacial polymerization of PIP and TMC. First, PES membrane substrate was exposed to an aqueous basic solution of PIP (2% w/v) for 2 min. Then, before exposure to hexane solutions containing 0.1% w/v TMC for 2 min, excessive PIP was removed from PIP-loaded substrates using a rubber roller. The resulting membrane was subsequently stored in DI water before testing.

2.4. Characterizations. The cloud points of different polymer solutions with different solvent systems were determined by a titrimetric method at room temperature. The homogeneous solution was prepared in a glass bottle. Water was added drop-by-drop into the homogeneous solution with stirring until the solution turned cloudy. The dope viscosity was tested using a viscometer (DV2T, Brookfield, USA).

The morphology of membranes was observed by a field-emission scanning electron microscope (FESEM, Hitachi S4800). Before observation, the membranes were freeze-dried and immersed in liquid nitrogen and subsequently fractured. Then, the samples were sputtered with gold prior to the observation.

The surface charge characteristics of the membranes after interfacial polymerization were studied by streaming potential measurements with an electrokinetic analyzer (SurPASS3, AntonPaar). A 1 mM KCl solution was circulated through adjustable measuring cell containing the membrane sample. Automatic titrations with 0.1 M HCl and 0.1 M NaOH were

DOI: 10.1021/acs.iecr.9b02217
Ind. Eng. Chem. Res. 2019, 58, 12280−12290

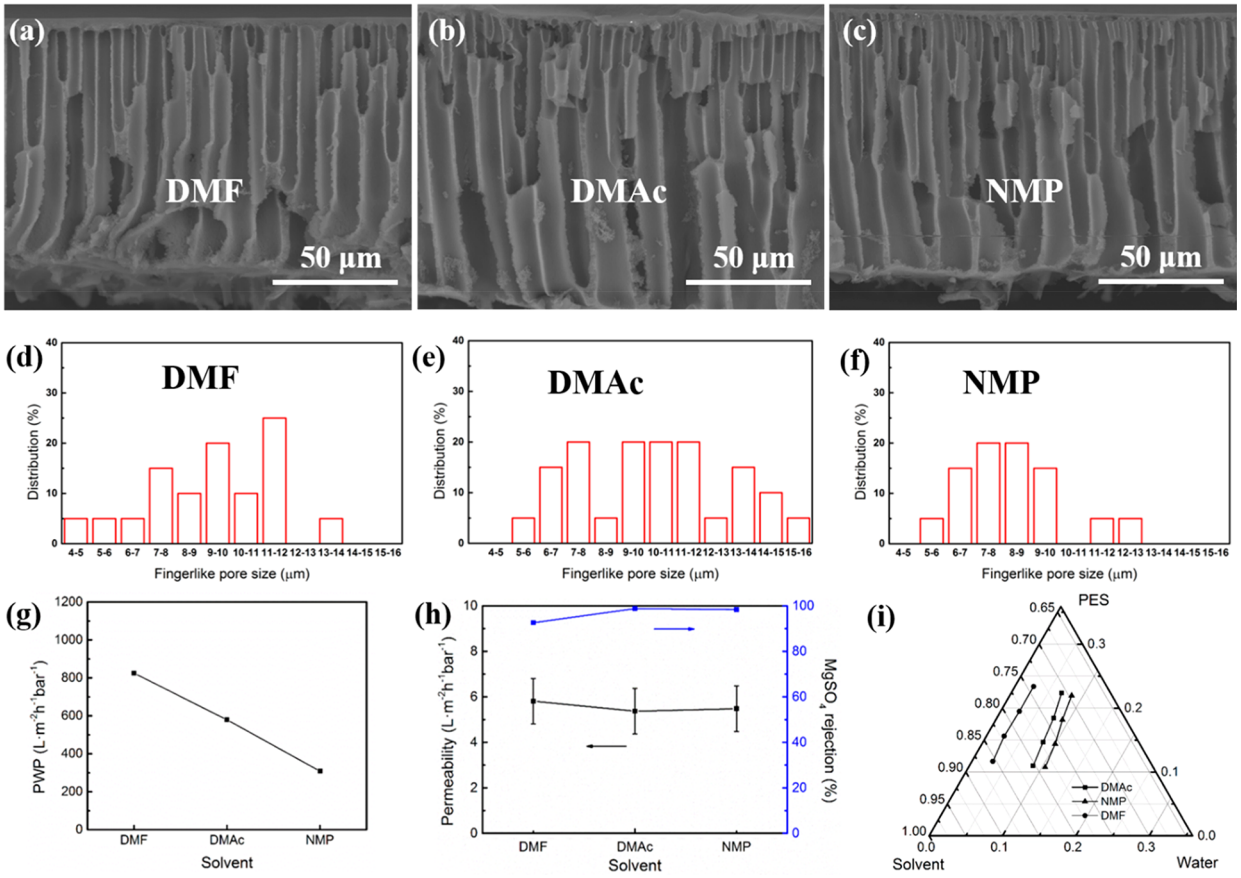

Figure 1. Effects of solvent types on (a–c) structure of substrates and (d–f) widths of the fingerlike macrovoids. Performance of (g) substrates and (h) TFC membranes. (i) Cloud point graph of different solvents.

carried out to study the pH dependence of the zeta potential and thus determine the isoelectric point with the method described previously.

2.5. Evaluation of Membrane Performance. The pure water permeability (PWP) of prepared membranes was tested in a dead-end permeation cell at a transmembrane pressure of 6 bar. Before test, membranes were conditioned with DI water at 6 bar for more than 10 min to ensure that the membrane reached a steady state. The PWP was measured from eq 1:

$$\mathrm{PWP} = \frac{Q}{\Delta P \times A} \tag{1}$$

where Q is the water permeation volumetric flow rate (L/h), A is the effective filtration area (m^2), and ΔP is the trans-membrane pressure (TMP) across the membrane (bar).

The single salt rejection and mixed salt separation performances were studied with a cross-flow system at a TMP of 6 bar and a constant temperature of 25 °C. For single salt rejection experiments, the feed was salt aqueous solution (1000 ppm) of four kinds of salts, and the conductivity of the raw liquid and the permeated liquid were measured with a conductivity meter (FE30, Mettler-Toledo). The rejection was calculated using eq 2:

$$R_T\ (\%) = \left(1 - \frac{c_p}{c_f}\right) \times 100 \tag{2}$$

where c_p and c_f are the solute concentrations in the permeate and the feed solution, respectively.

For mixed salt separation experiment, the feed was mixture of NaCl and Na_2SO_4 solutions with different concentration. The concentrations of feed and permeate solution were measured by an ion chromatography (Dionex, ICS-2000). The rejection and the separation factor were calculated using eqs 2 and 3 individually:

$$a = \frac{1 - R_{\mathrm{NaCl}}}{1 - R_{\mathrm{Na_2SO_4}}} \tag{3}$$

where R_{NaCl} and $R_{\mathrm{Na_2SO_4}}$ are the rejection rates of NaCl and Na_2SO_4 respectively.

To evaluate the chlorine resistance, H-TFC membranes were immersed in 1000 ppm of NaClO aqueous solution for certain time. After that, the membranes were taken out and washed with DI water. Subsequently, the permeation and rejection for 1000 ppm of Na_2SO_4 aqueous solution were tested.

3. RESULTS AND DISCUSSION

First, the design and fabrication conditions of the optimum substrate of H-TFC membranes are discussed. Then, the performance of H-TFC membranes is systematically characterized and compared with commercial membranes. Finally, the compressive strength, chlorine resistance, heat resistance, and long-term stability of H-TFC membrane, which are essential for applications in chlor-alkali industry, are investigated.

DOI: 10.1021/acs.iecr.9b02217
Ind. Eng. Chem. Res. 2019, 58, 12280–12290

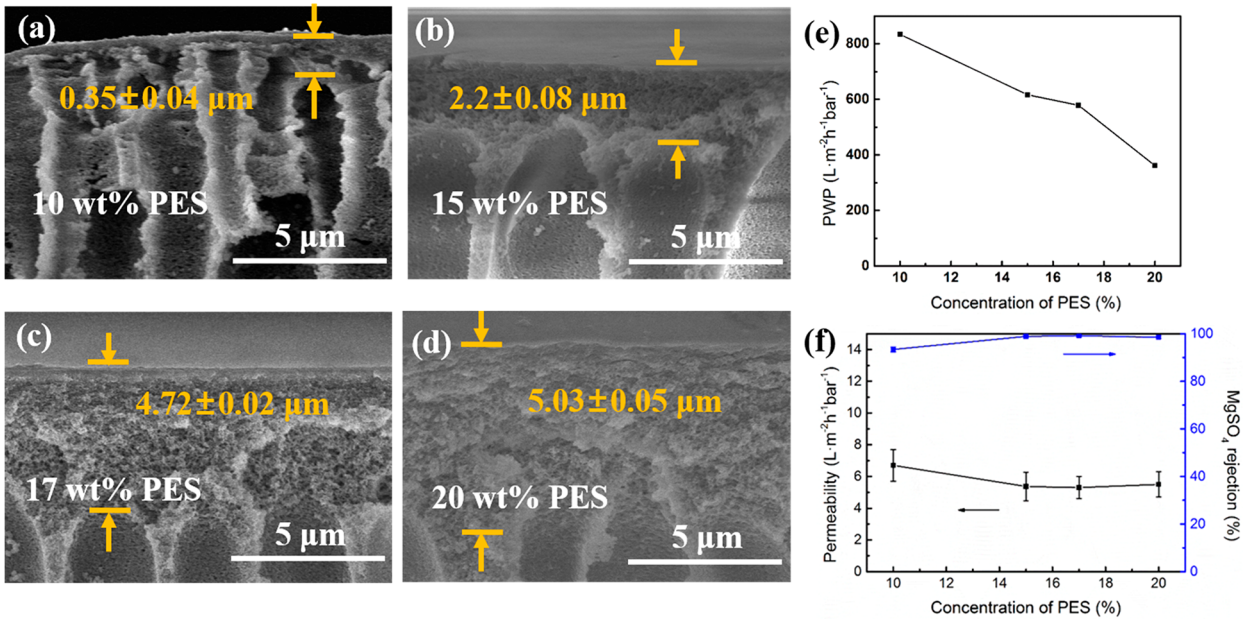

Figure 2. Effects of PES concentration on (a–d) structure of substrates and performance of (e) substrates and (f) TFC membranes, with fixed 40 wt % PEG concentration.

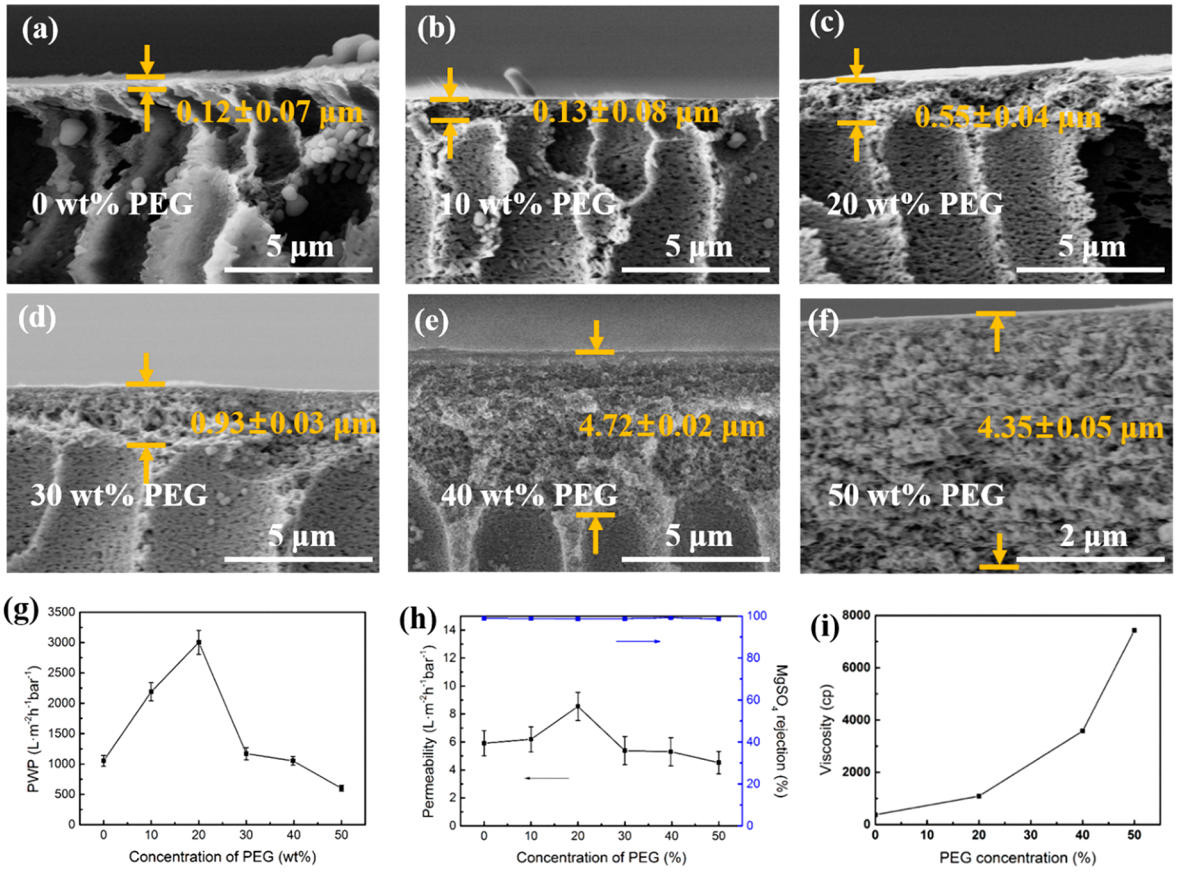

Figure 3. Effects of PEG concentration on (a–f) structure of substrates and performance of (g) substrates, and (h) TFC membranes, with fixed 17 wt % PES concentration. (i) Relationship between PEG concentration and dope viscosity.

3.1. Designing Substrate Structures for High-Performance NF Membranes. *3.1.1. Effects of Solvent Types.* During the NIPS process of polymeric membranes, the selection of solvents is crucial to the properties of the resultant membranes.[31] Herein, membranes were prepared with dopes containing different solvents (i.e., DMF, DMAc and NMP) at a composition of PES/PEG/solvent = 17.0/40.0/43.0 wt %. The SEM images of the substrates are shown in Figure 1a–c. There is no obvious difference among the three membranes. However, from Figure 1g,h, it can be noticed that the PWP

DOI: 10.1021/acs.iecr.9b02217
Ind. Eng. Chem. Res. 2019, 58, 12280–12290

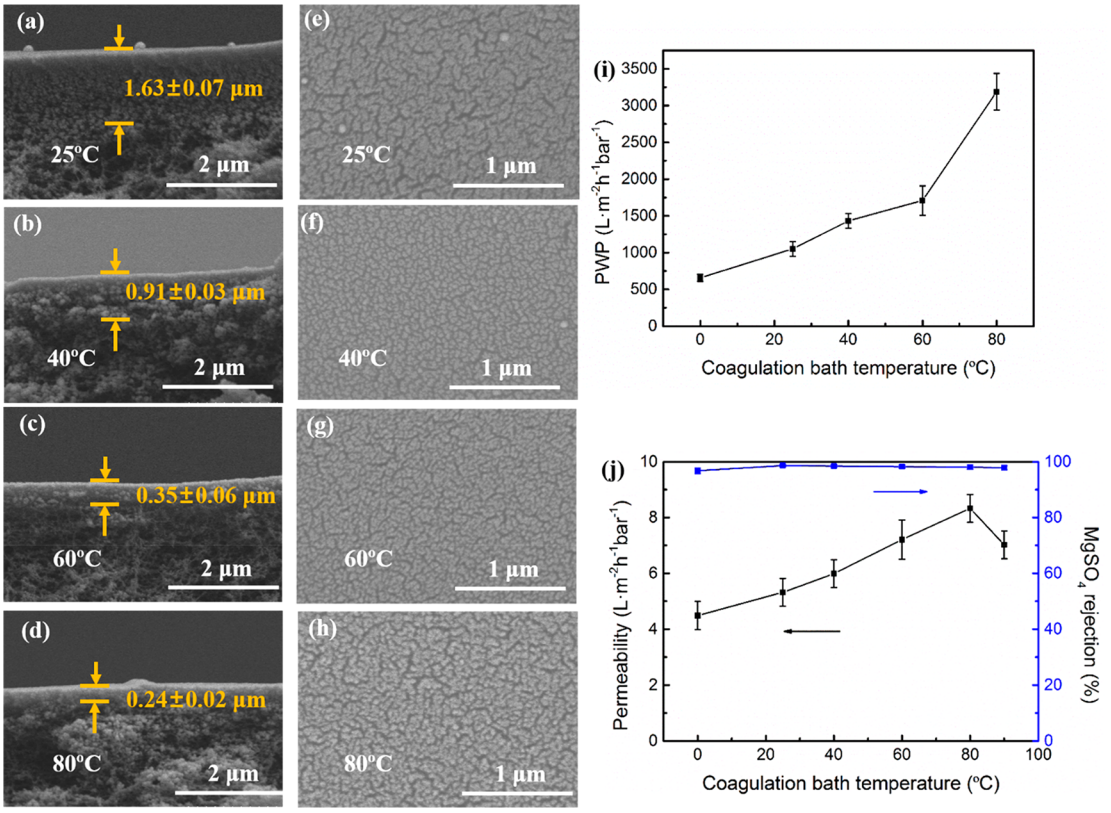

Figure 4. Effects of coagulation bath temperature on (a–d) structure and (e–h) surface of substrates, and performance of (i) substrates and (j) TFC membranes.

of the membranes follow the sequence of DMF > DMAc > NMP. Furthermore, the TFC membrane prepared from DMF has the lowest $MgSO_4$ rejection and the highest PWP.

The effects of solvent types on the substrate structure can be explained both thermodynamically and kinetically. During the NIPS process, a thermodynamically stable polymer solution has a tendency of liquid–liquid demixing. The cast solution is "phase-separated" into polymer-rich and polymer-lean phases, then nucleated and grows, when immersed in nonsolvent.[11] The thermodynamics and kinetics of this process can be explained by phase separation and mass transfer.[32] As shown in the ternary phase diagram (Figure 1i), a relatively minimum gap exists between the cloud-point curve of PES/DMF solution and the polymer/solvent axis among the three studied solution containing DMF, DMAc, and NMP. This indicates the PES/DMF dope experiences the most rapid phase transition rate which results in a loose dense selective layer.[33,34] By contrast, the transition process of PES/NMP dope takes the longest time, leading to a dense selective layer. In addition, according to the ternary phase diagram, the component of dope is over the critical solvent point. This means that during the immersion precipitation process the lean-phase micronucleus forms in the dope solution prior to liquid–liquid demixing. Therefore, the window of solvent/nonsolvent exchange can be broadened before demixing occurs, resulting in the formation of fingerlike pores. In terms of kinetics, Xia et al. calculated the diffusion coefficients of the solvents in water, which follows the trend of NMP < DMAc < DMF.[35] The widths of the fingerlike macrovoids across the cross-section of the substrates were measured and statistically analyzed. From the results shown in Figure 1d–f, the substrates with DMF and NMP as solvents possess largest and narrowest macrovoids, respectively. However, the substrate with DMAc as solvent exhibits a combination of large and narrow macrovoids. Both contribute for low resistance water transportation. Therefore, the as-mentioned PES/PEG/DMAc dope solution was chosen as dope solution for further study.

3.1.2. Effects of Polymer Concentration. The polymer concentration of dope solution would affect the structure of substrate and the performance of TFC membranes. In each experiment, 40 wt % PEG 400 was used as additive to preserve pore connectivity. According to Figure 2a–d, we can see that with the increase of PES concentration from 10 to 20%, the thickness of the spongy layer increases from 0.35 to 5.03 μm. As shown in Figure 2e,f, with the increase of polymer concentration, the PWP of substrate declines gradually. For the TFC membrane, the $MgSO_4$ rejection of TFC membrane increases when the PES concentration increases from 10 to 15% and remains stable when the concentration is higher than 15%. On the contrary, the permeability has the opposite trend.

The phenomenon is consistent with the membrane formation mechanisms involving instant and delayed demixing.[36] As the PES concentration of dope rises, polymer molecules are enriched at the membrane surface, which leads to lower porosity of the skin layer. Therefore, the exchange rate of solvent and nonsolvent decreases, while the time of delayed demixing is increased. Furthermore, the formation of macrovoids is suppressed, which results in a thicker spongy layer. Thus, to get a high-performance TFC membrane, 17% was chosen as PES concentration for further study.

3.1.3. Effects of PEG Concentration. The addition of PEG not only improves the hydrophilicity of membranes but also induce more porous structure.[37] As can be observed from

DOI: 10.1021/acs.iecr.9b02217
Ind. Eng. Chem. Res. 2019, 58, 12280–12290

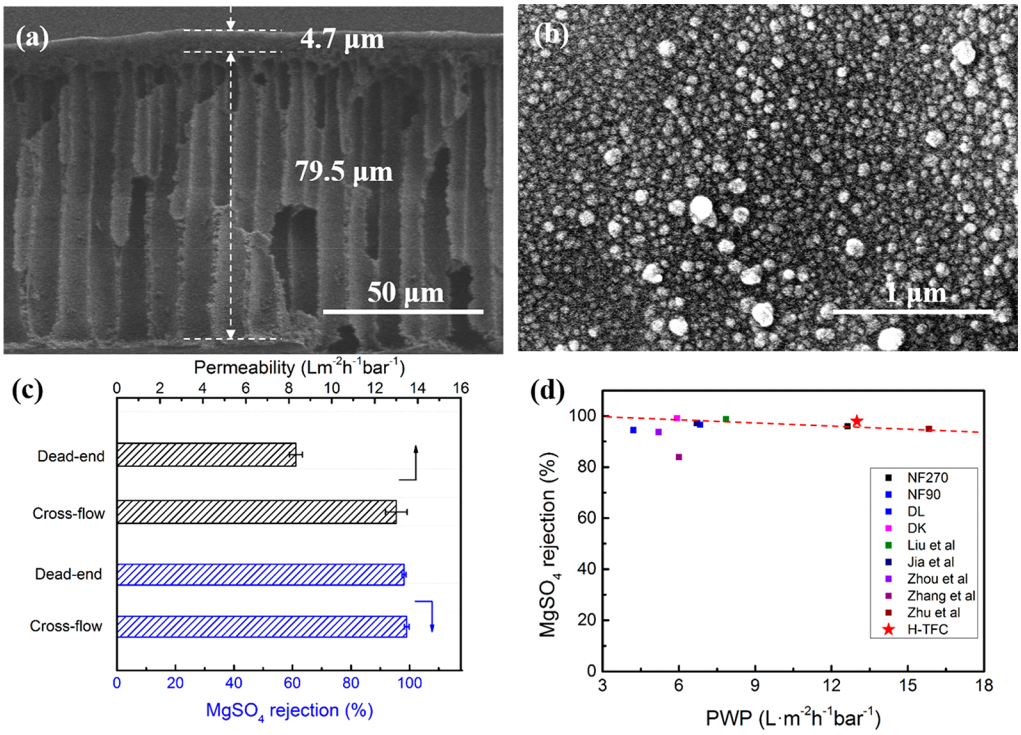

Figure 5. Morphology of the H-TFC membranes: (a) cross section, (b) surface. (c) Performance of H-TFC membrane with dead-end and cross-flow experiments, respectively. (d) Trade-off line of TFC NF membranes.

Figure 3a–f, the thickness of spongy layer grows from 0.12 to 4.35 μm, with the increase of PEG concentration from 0 to 50%. Furthermore, the spongy layer thickness of membrane with 40% PEG is almost 5 times as thick as that containing 30%. Besides, the permeability of both substrates and TFC membranes increases as the PEG concentration increases from 0 to 20% and declines slightly as concentration rises from 30 to 40%. However, the PWP of TFC membranes decrease sharply when concentration is larger than 40% with a steady $MgSO_4$ rejection above 98.7% (Figure 3g,h).

This fact can be attributed to the effect PEG has on the hydrophilicity and viscosity of dope simultaneously. The hydrophilic PEG works as a nonsolvent additive that encourages the mechanism of phase inversion transit from delayed demixing to instantaneous demixing, which consequently promotes the formation of fingerlike macrovoid structures, so the width of fingerlike pores increases with the increase of PEG concentration from 0 to 20%, leading to the enhancement of PWP of substrate and TFC membrane.[38] In addition, the dope viscosity with different PEG concentrations is tested (Figure 3i), which grows from 485 to 7510 cP and increases sharply with PEG concentration from 20 to 50%. Thus, the exchange rate of solvent and nonsolvent declines, while the time of delayed demixing is increased, leading to the dramatic increase of the thickness of the spongy layer. Then, the PWP of membrane decreases, though the hydrophilicity of membrane is improved. The PEG concentration of 40% was chosen for its high permeability and the sufficient thickness of spongy layer.

3.1.4. Effects of Coagulation Bath Temperature. The NIPS process can also be effected by the condition of coagulation, and controlling the coagulation bath temperature is an easy-operating and environment friendly method.[39] Figure 4a–d and 4e–h show the SEM images of the membranes' cross section and surface, respectively, prepared with different coagulation bath temperatures. From these, the spongy layer thickness of these membranes is similar. However, the skin layer thickness declines with the increase of coagulation bath temperature. The surface pores structures are similar when the bath temperature increases from 25 to 60 °C and become loose when it is 80 °C. Beyond that, the PWP of substrate and H-TFC increase with the temperature from 20 to 80 °C, and the $MgSO_4$ rejection remains above 95% (Figure 4i,j).

Under the guidance of nucleation and growth mechanism, as the affinity between DMAc and water is strong enough, the out-diffusion rate of DMAc is much higher than the in-diffusion rate of water, which results in dense skin layer,[40] so a lower diffusion rate for water into the sublayer leads to fewer nuclei and possibly promotes the formation of macrovoids. With the higher bath coagulation temperature, the diffusion rates of DMAc and water at the interface are accelerated.[41] Therefore, precipitation is improved, contributing to the less-dense skin layer and loose surface pores. Hence, to obtain a high-performance membrane, we chose 80 °C as the coagulation bath temperature.

On the basis of the above investigations, the optimized conditions for fabricating H-TFC membrane were as follows: PES/PEG 400/DMAc = 17 wt %/40 wt %/43 wt %, coagulation bath temperature was 80 °C; cross section and surface pictures of the prepared membrane are shown in Figure 5a,b. The membrane contains a substrate with a large amount of loose fingerlike pores and a spongy layer with sufficiently high thickness. In addition, the surface exhibits intensive nodules which can improve the pure water permeability.[42] The PWPs of obtained membranes with dead-end and cross-flow operations were 8.3 and 13.0 L m^{-2} h^{-1} bar^{-1}, while the $MgSO_4$ rejections were 98.1 and 99.0%, respectively (Figure

DOI: 10.1021/acs.iecr.9b02217
Ind. Eng. Chem. Res. 2019, 58, 12280–12290

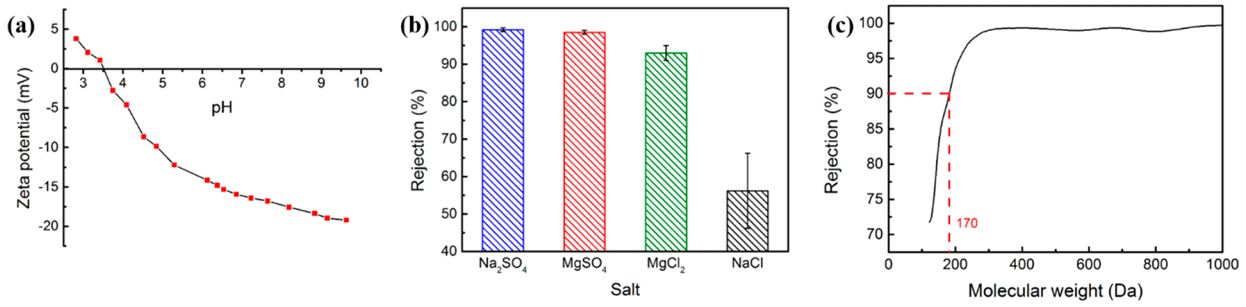

Figure 6. (a) Zeta-potential of H-TFC NF membrane. Experiments were carried out with 1 mM KCl. (b) Rejection of four types of common salts of H-TFC membranes. (c) MWCO of H-TFC membranes.

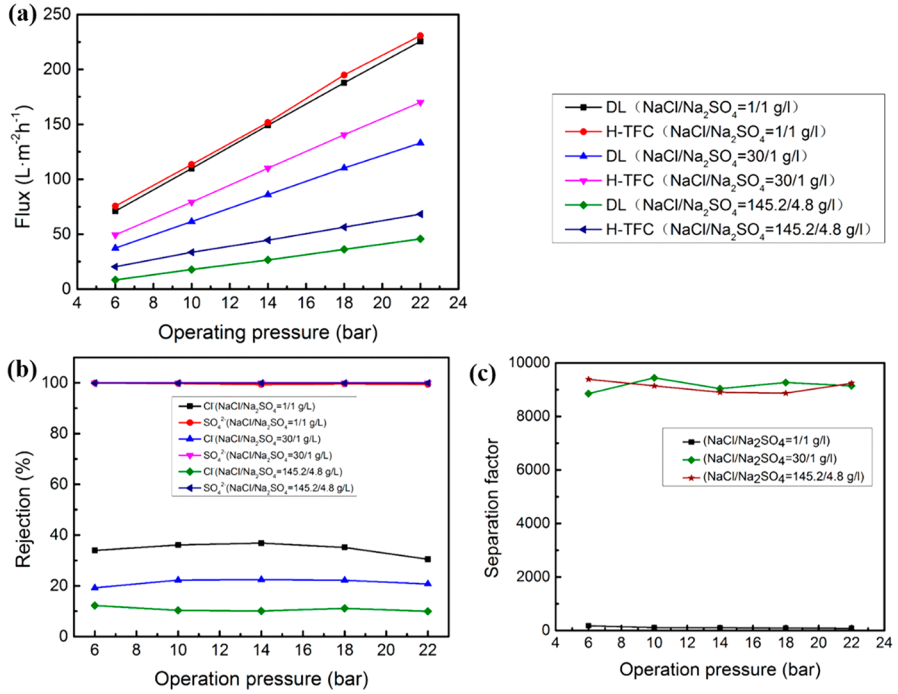

Figure 7. (a) Flux of H-TFC and DL membranes with different salt concentrations. (b) Rejection and (c) separation factor of SO_4^{2-} and Cl^- of H-TFC.

5c). Furthermore, the performance of H-TFC membranes breaks the trade-off effect of most state-of-art NF membranes under the cross-flow filtration operation (Figure 5d).

3.2. Performance of TFC Membranes. *3.2.1. Rejection of Single Salts.* Before detecting the single salt rejections, the surface zeta potential of H-TFC membrane was measured. The isoelectric point of TFC membrane was about 3.5 (Figure 6a), above which the membrane was negatively charged. Then, a series of single salt rejection tests ($MgSO_4$, $MgCl_2$, Na_2SO_4, and NaCl) was conducted. As shown in Figure 6b, the following order of the salt rejection was observed: Na_2SO_4 > $MgSO_4$ > $MgCl_2$ > NaCl. The result can be explained by the Donnan exclusion and steric effects. The fact that H-TFC membrane has higher rejections for $MgSO_4$ and Na_2SO_4 than chloride salt is attributed to the negatively charged membrane surface. The higher rejection of $MgCl_2$ than NaCl may be due to the narrow pore size of H-TFC membrane, which was tested by PEGs with various molecular weights (Figure 6c). The pore size of H-TFC membrane is calculated from the molecular weight cutoff (MWCO) by eq 4:[43]

$$\log r_n = -1.32 + 0.395 \log \mathrm{MWCO} \quad (4)$$

where r_n is the nominal pore radius of the membrane, with units of nm for r_n and g/mol for MWCO. The nominal pore radius of H-TFC membrane was about 0.364 nm, which was larger than hydrated sodium ion (0.358 nm) but smaller than hydrated magnesium ion (0.428 nm).[44]

3.2.2. Separation of SO_4^{2-} and Cl^-. In order to test the separation performance of H-TFC membranes in the chlor-alkali industry, a series of experiments were done with different salt concentrations (Na_2SO_4/NaCl = 1/1, 1/30, 4.8/145.2 g/L) under operating pressures from 6 to 22 bar. Meanwhile, the comparative test of commercial DL membranes was carried out. Figure 7a displays the flux of H-TFC and DL membranes under various salt concentration and TMP. The following phenomena could be observed from the test: (1) The flux of both H-TFC membrane and DL membrane decreased gradually with the increase of salt concentration, as normally observed for high-salinity induced concentration polarization. (2) The flux of them grow almost linearly with the raise of TMP, which is due to enhanced driving force. (3) The H-TFC membrane shows substantially higher flux than do DL membranes at elevated salt concentrations, which is mainly because of the specially designed substrate that provides

DOI: 10.1021/acs.iecr.9b02217
Ind. Eng. Chem. Res. 2019, 58, 12280−12290

minimum water transport resistance, low tendency for concentration polarization, and minimum sacrifice of the separation and mechanical properties of the TFC membranes.

Furthermore, the separation performance of H-TFC membrane was tested, as shown in Figure 7b. The membrane has stable retention of the sulfate and chloride ions under various pressures from 6 to 22 bar. Besides, dealing with higher salt concentration system, the H-TFC membrane has steady rejection of sulfate and lower rejection of chloride ions. This is probably attributed to the fact that with the increase of salt concentration the concentration difference between the sides of the membrane rises and the diffusion rate of ions is enhanced. However, sulfate is retained due to the narrow nominal pore size of H-TFC, which is larger than chloride (0.332 nm) and smaller than sulfate (0.379 nm). In addition, the transition between permanent (pore-flow) and transient (solution-diffusion) free-volume elements exists in the H-TFC membranes, which can improve the separation performance of NaCl and Na_2SO_4 combining the pore-flow and solution-diffusion mechanism.[45] Following that, the separation factor of NaCl and Na_2SO_4 was calculated (Figure 7c). The separation factor of H-TFC membrane increased sharply with the increase of salt concentration, as a result of the improved diffusion rate of chloride ions. When the total salt concentration was 150 g/L, the separation factor was over 9000, which showed a great application prospect in future for chlor-alkali, brine refining and other industries involving high-salinity solutions separations.

3.3. Stability of Nanofiltration Membranes for Application in Chlor-Alkali Process. *3.3.1. Compressive Strength.* The deformation problem of membrane structure under high pressure often causes performance decline. So the compressive strength of membranes is very significant for practical application. The compressive strength test of H-TFC membrane was conducted by a hysteresis cross-flow test. As shown in Figure 8, the flux keeps very stable during a 1.5 testing cycle with the applied hydraulic pressure ranging from 6 to 22 bar, so the possibility for practical application of H-TFC membrane is confirmed after the compressive strength test.

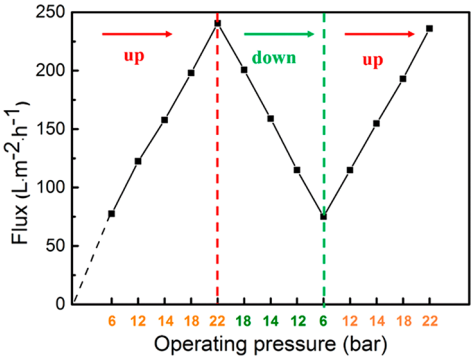

Figure 8. Pressure test of H-TFC membranes.

3.3.2. Chlorine Resistance. Active chlorine existing in the chlor-alkali process can destroy the PA layer on TFC membrane surface and affects the performance of TFC membranes. The chlorine resistance test of traditional MPD-TMC TFC and H-TFC membranes were conducted after immersing in 1000 ppm of NaClO aqueous solution for certain time. The PWP of traditional MPD-TMC TFC increased from 5.5 to 9.9 L m^{-2} h^{-1} bar^{-1}, and the $MgSO_4$ rejection decreased from 98.0 to 70.0% after only 1 h of NaClO treatment. By comparison, the PWP of H-TFC membrane increased from 7.8 to 10.0 L m^{-2} h^{-1} bar^{-1}, and the $MgSO_4$ rejection decreased from 98.0 to 86.1% after 50 h of NaClO treatment (Figure 9**a**-**b**). The chlorine resistance of H-TFC membrane was improved, compared with traditional MPD-TMC TFC membrane. The result can be explained by the mechanism of a chlorine erosion of PA layer. In the contact of chlorine and PA layer, chlorine attacks the active amidic hydrogen linked to aromatic ring, while the destruction of the membrane chemical structure leads to the loss of separation performance.[30] In this work, PIP was chosen as the amine monomer, thanks to its lack of secondary amines and stable performance in free chlorine system, rather than the MPD with primary amines (Figure 9c,d). In addition, the nominal pore radius of H-TFC membrane is 0.364 nm can prevent ClO^- entering the inner of interfacial polymerization layer.

3.3.3. Heat Resistance. For the application of H-TFC membrane in the high-salinity solution separation process of the chlor-alkali industry, the heat resistance test of H-TFC membrane was undertaken, and the results compared with those of the DL membrane (Figure 10). Under the temperatures from 25 to 55 °C, the flux of both membranes increased almost linearly because the viscosity of water declined with the increase of temperature. Besides, the rejection of sulfate and chloride remained stable for both membranes. It is noteworthy that the flux of H-TFC membrane is higher than that of DL membrane, which is mainly attributed to the low transport resistance of the specially designed substrate, as elaborated in earlier sections. This confirms the possibility of H-TFC membrane to be applied in the system from 25 to 55 °C.

3.3.4. Long-Term Performance. Long-term permeation tests were also conducted to investigate the performance stability of the H-TFC membranes, and the results are shown in Figure 11. During the test, the changes of the flux and rejection during 168 h continuous filtration of 1000 ppm of Na_2SO_4 solution were obtained. From Figure 11, it is clear that both the Na_2SO_4 rejection (above 99%) and flux (around 9.3 L m^{-2} h^{-1} bar^{-1}) are stable. In short, the result of long-term tests indicates that the H-TFC membrane shows good durability, which is meaningful to the potential application in the chlor-alkali industry.

4. CONCLUSIONS

High-performance NF membranes, "H-TFC", were achieved with the following strategies: (1) The optimized substrate was achieved with the dope composition at PES/PEG 400/DMAc = 17 wt %/40 wt %/43 wt % with the coagulation bath temperature at 80 °C. The resultant substrate possesses the best ratio of the spongy and fingerlike layers, which not only provides a low resistance transport channel to improve the membrane permeability but also ensures enough strength to treat high-salinity solutions. The H-TFC membranes own a high pure water permeability (13.0 L m^{-2} h^{-1} bar^{-1}) and excellent compressive strength which is proved through the pressure test and the flux is linear with pressure from 6 to 22 bar. (2) The 0.364 nm nominal pore size of the finely tuned membrane can realize the separation of Cl^- and SO_4^{2-} at a relatively high level (separation factor about 9000).

The H-TFC membrane also possesses excellent long-term stability and reasonable resistance toward chlorine and heat. Therefore, the H-TFC membranes have great potential

DOI: 10.1021/acs.iecr.9b02217
Ind. Eng. Chem. Res. 2019, 58, 12280−12290

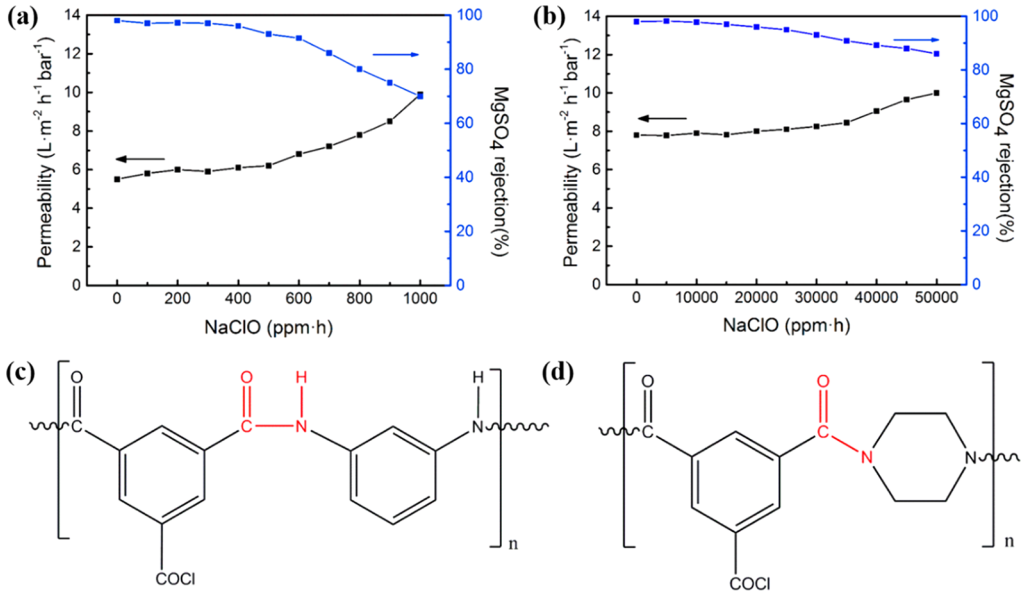

Figure 9. Chlorine resistance of (a) traditional MPD-TMC TFC membranes and (b) H-TFC membranes. (c) Molecular structures of MPD-TMC polyamide and (d) PIP-TMC polyamide.

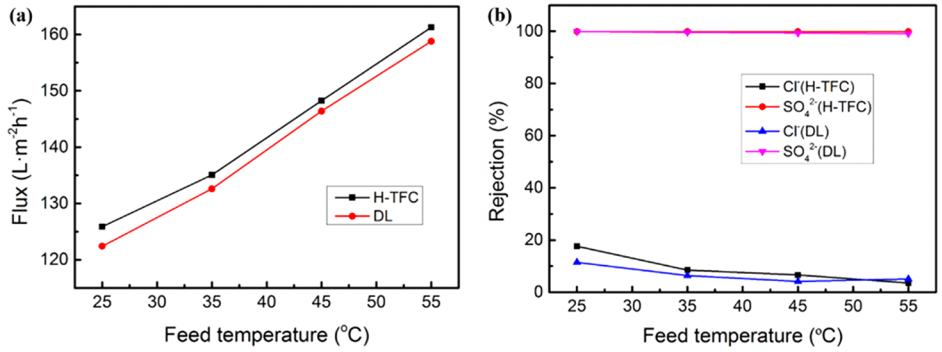

Figure 10. Heat resistance test of H-TFC membranes. Feed solution concentration: $NaCl/Na_2SO_4$ = 145.2/4.8 g/L; pressure: 22 bar.

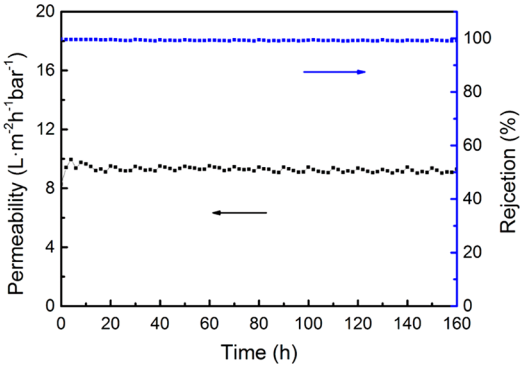

Figure 11. Long-term stability experiment of H-TFC membranes. Feed solution concentration: 1000 ppm of Na_2SO_4; pressure: 22 bar.

application in high-salinity solutions separation of chlor-alkali and other industries.

AUTHOR INFORMATION

Corresponding Author

*E-mail: ssp@njtech.edu.cn. Tel.: +86-25-83587560.

ORCID

Yi-Qun Fan: 0000-0002-2455-8979

Shi-Peng Sun: 0000-0002-6849-2473

Notes

The authors declare no competing financial interest.

ACKNOWLEDGMENTS

We gratefully acknowledge the research funding provided by National Natural Science Foundation of China (21878146), Jiangsu Provincial Department of Human Resources and Social Security (JNHB-040), and the State Key Laboratory of Materials-Oriented Chemical Engineering (ZK201608). S.-P.S. is supported by the program of "Thousand Talents Plan-Distinguished Young Professor".

REFERENCES

(1) Pernetti, M.; Di Palma, L. Experimental evaluation of inhibition effects of saline wastewater on activated sludge. *Environ. Technol.* **2005**, *26* (6), 695−704.

(2) Zhao, D. f.; Xue, J. l.; Li, S.; Sun, H.; Zhang, Q. D. Theoretical analyses of thermal and economical aspects of multi-effect distillation desalination dealing with high-salinity wastewater. *Desalination* **2011**, *273*, 292−298.

(3) Crook, J.; Mousavi, A. The chlor-alkali process: A review of history and pollution. *Environ. Forensics* **2016**, *17* (3), 211−217.

(4) Barr, A. Sulphate removal by nanofiltration. *Filtr. Sep.* **2001**, *38* (6), 18−20.

DOI: 10.1021/acs.iecr.9b02217
Ind. Eng. Chem. Res. 2019, 58, 12280−12290

(5) Yan, Z. Q.; Zeng, L. M.; Li, Q.; Liu, T. Y.; Matsuyama, H.; Wang, X. L. Selective separation of chloride and sulfate by nanofiltration for high saline wastewater recycling. *Sep. Purif. Technol.* **2016**, *166* (2016), 135−141.
(6) Pérez-González, A.; Urtiaga, A. M.; Ibáñez, R.; Ortiz, I. State of the art and review on the treatment technologies of water reverse osmosis concentrates. *Water Res.* **2012**, *46* (2), 267−283.
(7) Madaeni, S. S.; Kazemi, V. Treatment of saturated brine in chlor-alkali process using membranes. *Sep. Purif. Technol.* **2008**, *61* (1), 68−74.
(8) Liang, C. Z.; Sun, S. P.; Li, F. Y.; Ong, Y. K.; Chung, T. S. Treatment of highly concentrated wastewater containing multiple synthetic dyes by a combined process of coagulation/flocculation and nanofiltration. *J. Membr. Sci.* **2014**, *469* (2014), 306−315.
(9) Li, Q.; Cao, B.; Li, P. Fabrication of High Performance Pervaporation Desalination Composite Membranes by Optimizing the Support Layer Structures. *Ind. Eng. Chem. Res.* **2018**, *57* (32), 11178−11185.
(10) Zhao, Y.; Li, Y.; Yuan, S.; Zhu, J.; Houtmeyers, S.; Li, J.; Dewil, R.; Gao, C.; Van der Bruggen, B. A chemically assembled anion exchange membrane surface for monovalent anion selectivity and fouling reduction. *J. Mater. Chem. A* **2019**, *7*, 6348−6356.
(11) Schafer, A. I.; Fane, A. G.; Waite, T. D. *Nanofiltration: Principles and Applications*. Elsevier Advanced Technology: New York, 2005.
(12) Mohammad, A. W.; Teow, Y. H.; Ang, W. L.; Chung, Y. T.; Oatleyradcliffe, D. L.; Hilal, N. Nanofiltration membranes review: Recent advances and future prospects. *Desalination* **2015**, *356* (2015), 226−254.
(13) Colburn, A. S.; Meeks, N.; Weinman, S. T.; Bhattacharyya, D. High Total Dissolved Solids Water Treatment by Charged Nanofiltration Membranes Relating to Power Plant Applications. *Ind. Eng. Chem. Res.* **2016**, *55* (14), 4089−4097.
(14) Raman, L. P.; Cheryan, M.; Rajagopalan, N. Consider nanofiltration for membrane separations. *Chem. Eng. Prog.* **1994**, *90* (3), 68−75.
(15) Hilal, N.; Al-Zoubi, H.; Darwish, N. A.; Mohamma, A. W.; Abu Arabi, M. A comprehensive review of nanofiltration membranes:-Treatment, pretreatment, modelling, and atomic force microscopy. *Desalination* **2004**, *170* (3), 281−308.
(16) Du, F.; Warsinger, D. M.; Urmi, T. I.; Thiel, G. P.; Kumar, A.; Lienhard V, J. H. Sodium Hydroxide Production from Seawater Desalination Brine: Process Design and Energy Efficiency. *Environ. Sci. Technol.* **2018**, *52* (10), 5949−5958.
(17) Xie, L. Y.; Nie, F.; He, G. H.; Tan, M.; Feng, J. H. Gas Separation and Mechanical Performance of PAN/CA Blend Composite Membranes. *Polymer. Mater. Sci. Eng.* **2011**, *27* (7), 95−97.
(18) Kim, S. H.; Lee, T. M. Performance improvement of membrane distillation using carbon nanotubes. *Membr. Water. Treat.* **2016**, *7* (4), 367−375.
(19) Li, Y.; Xue, J. J.; Zhang, X.; Cao, B.; Li, P. Formation of macrovoid-free PMDA-MDA polyimide membranes using a gelation-NIPs method for organic solvent nanofiltration. *Ind. Eng. Chem. Res.* **2019**, *58*, 6712−6720.
(20) Xu, S.; Zhang, H.; Yu, F.; Zhao, X. X.; Wang, Y. Enhanced ethanol recovery of PDMS mixed matrix membranes with hydrophobically modified ZIF-90. *Sep. Purif. Technol.* **2018**, *206*, 80−89.
(21) Wang, K. Y.; Chung, T. S.; Rajagopalan, R. Novel Polybenzimidazole (PBI) Nanofiltration Membranes for the Separation of Sulfate and Chromate from High Alkalinity Brine To Facilitate the Chlor-Alkali Process. *Ind. Eng. Chem. Res.* **2007**, *46* (2017), 1572−1578.
(22) Feng, Y.; Shamsaei, E.; Davies, C. H. J.; Wang, H. Inorganic particle enhanced polymer hollow fiber membranes with high mechanical properties. *Mater. Chem. Phys.* **2015**, *167* (2015), 209−218.
(23) Elkhaldi, R. M.; Guclu, S.; Koyuncu, I. Enhancement of mechanical and physical properties of electrospun PAN nanofiber membranes using PVDF particles. *Desalin. Water Treat.* **2016**, *57* (54), 26003−26013.
(24) Di Vona, M. L.; Sgreccia, E.; Donnadio, A.; Casciola, M.; Chailan, J. F.; Auer, G.; Knauth, P. Composite polymer electrolytes of sulfonated poly-ether-ether-ketone (SPEEK) with organically functionalized TiO_2. *J. Membr. Sci.* **2011**, *369* (1), 536−544.
(25) Lu, T. D.; Chen, B. Z.; Wang, J.; Jia, T. Z.; Cao, X. L.; Wang, Y.; Xing, W.; Lau, C. H.; Sun, S. P. Electrospun nanofiber substrates that enhance polar solvent separation from organic compounds in thin-film composites. *J. Mater. Chem. A* **2018**, *6* (31), 15047−15056.
(26) Heydari, M.; Moheb, A.; Ghiaci, M.; Masoomi, M. Effect of cross-linking time on the thermal and mechanical properties and pervaporation performance of poly(vinyl alcohol) membrane cross-linked with fumaric acid used for dehydration of isopropanol. *J. Appl. Polym. Sci.* **2012**, *128* (3), 1640−1651.
(27) Wang, K. Y.; Chung, T. S.; Qin, J. J. Polybenzimidazole (PBI) nanofiltration hollow fiber membranes applied in forward osmosis process. *J. Membr. Sci.* **2007**, *300* (1), 6−12.
(28) Yang, Y. N.; Zhang, H. X.; Wang, P.; Zheng, Q. Z.; Li, J. The influence of nano-sized TiO_2 fillers on the morphologies and properties of PSF UF membrane. *J. Membr. Sci.* **2007**, *288* (1-2), 231−238.
(29) Sun, S. P.; Hatton, T. A.; Chung, T. S. Hyperbranched polyethyleneimine induced cross-linking of polyamide-imide nanofiltration hollow fiber membranes for effective removal of ciprofloxacin. *Environ. Sci. Technol.* **2011**, *45* (9), 4003−9.
(30) Cheng, X. Q.; Liu, Y.; Guo, Z.; Shao, L. Nanofiltration membrane achieving dual resistance to fouling and chlorine for "green" separation of antibiotics. *J. Membr. Sci.* **2015**, *493* (2015), 156−166.
(31) Altena, F. W.; Smolders, C. A. Calculation of liquid-liquid phase separation in a ternary system of a polymer in a mixture of a solvent and nonsolvent. *Macromolecules* **1982**, *15* (6), 1491−1497.
(32) Guillotin, M.; Lemoyne, C.; Noel, C.; Monnerie, L. Physicochemical processes occurring during the formation of cellulose diacetate membranes. Research of criteria for optimizing membrane performance. IV. Cellulose diacetate-acetone-organic additive casting solutions. *Desalination* **1977**, *21* (2), 165−181.
(33) Sun, S. P.; Wang, K. Y.; Peng, N.; Hatton, T. A.; Chung, T. S. Novel polyamide-imide/cellulose acetate dual-layer hollow fiber membranes for nanofiltration. *J. Membr. Sci.* **2010**, *363* (1−2), 232−242.
(34) Jia, T. Z.; Lu, J. P.; Cheng, X. Y.; Xia, Q. C.; Cao, X. L.; Wang, Y.; Xing, W. H.; Sun, S. P. Surface enriched sulfonated polyarylene ether benzonitrile (SPEB) that enhances heavy metal removal from polyacrylonitrile (PAN) thin-film composite nanofiltration membranes. *J. Membr. Sci.* **2019**, *580* (2019), 214−223.
(35) Xia, Q. C.; Wang, J.; Wang, X.; Chen, B. Z.; Guo, J. L.; Jia, T. Z.; Sun, S. P. A hydrophilicity gradient control mechanism for fabricating delamination-free dual-layer membranes. *J. Membr. Sci.* **2017**, *539* (2017), 392−402.
(36) van de Witte, P. V.; Dijkstra, P. J.; van den Berg, J. W. A.; Feijen, J. Phase separation processes in polymer solutions in relation to membrane formation. *J. Membr. Sci.* **1996**, *117* (1996), 1−31.
(37) Ma, Y. X.; Shi, F. M.; Ma, J.; Wu, M. N.; Zhang, J.; Gao, C. J. Effect of PEG additive on the morphology and performance of polysulfone ultrafiltration membranes. *Desalination* **2011**, *272* (1), 51−58.
(38) Idris, A.; Yet, L. K. The effect of different molecular weight PEG additives on cellulose acetate asymmetric dialysis membrane performance. *J. Membr. Sci.* **2006**, *280* (1), 920−927.
(39) Wang, X. Y.; Zhang, L.; Sun, D. H.; An, Q. F.; Chen, H. F. Effect of coagulation bath temperature on formation mechanism of poly(vinylidene fluoride) membrane. *J. Appl. Polym. Sci.* **2008**, *110* (3), 1656−1663.
(40) Alexandridis, P.; Alan Hatton, T. Poly(ethylene oxide) poly(propylene oxide) poly(ethylene oxide) block copolymer surfactants in aqueous solutions and at interfaces: thermodynamics,

DOI: 10.1021/acs.iecr.9b02217
Ind. Eng. Chem. Res. 2019, 58, 12280−12290

structure, dynamics, and modeling. *Colloids Surf., A* **1995**, *96* (1−2), 1−46.
(41) Peng, J. M.; Su, Y. L.; Chen, W. J.; Shi, Q.; Jiang, Z. Y. Effects of Coagulation Bath Temperature on the Separation Performance and Antifouling Property of Poly(ether sulfone) Ultrafiltration Membranes. *Ind. Eng. Chem. Res.* **2010**, *49*, 4858−4865.
(42) Tan, Z.; Chen, S.; Peng, X.; Zhang, L.; Gao, C. Polyamide membranes with nanoscale Turing structures for water purification. *Science* **2018**, *360*, 518−521.
(43) Bowen, W. R.; Mukhtar, H. Characterisation and prediction of separation performance of nanofiltration membranes. *J. Membr. Sci.* **1996**, *112* (2), 263−274.
(44) Nightingale, E. R. Phenomenological theory of ion solvation. Effective radii of hydrated ions. *J. Phys. Chem.* **1959**, *63* (1959), 1381−1388.
(45) Wijmans, J. G.; Baker, R. W. The solution-diffusion model: a review. *J. Membr. Sci.* **1995**, *107* (1995), 1−21.

DOI: 10.1021/acs.iecr.9b02217
Ind. Eng. Chem. Res. 2019, 58, 12280−12290